FUNDAMENTAL STUDIES OF ACTIVE DIMPLES

Sébastien Lambert, Beverley J. McKeon,
Henrik Koberg and Jonathan F. Morrison
Department of Aeronautics,
Imperial College
London, SW7 2AZ, UK
j.morrison@imperial.ac.uk

ABSTRACT

The effect of local time-dependent dimple forcing of laminar channel and boundary-layer flow is investigated. Simulations of channel flow with a linearized boundary condition (no separation) for the dimple show how it generates streamwise vorticity and that, as the frequency of forcing increases, progressively more of the vorticity flux is generated by the local surface acceleration as opposed to the pressure-gradient mechanisms operating in the case of a static dimple. Flow visualization in a laminar boundary layer with small-amplitude dimple forcing over a range of frequencies shows that, at quite low frequencies, an inner horseshoe vortex is generated by surface pressure gradients, producing common flow away from the surface along the streamwise horizontal centre-line. At higher frequencies, an increase in viscous blockage leads to the formation of an outer horseshoe vortex, in addition to the inner one to which it rotates in the opposite sense. There are therefore two regions of common flow towards the surface, each one outboard of, and immediately adjacent to, the streamwise legs of the inner horseshoe. The region of common flow away from the surface within the inner horseshoe persists. At the two highest frequencies, the leading edge of the outer horseshoe has more or less broken up into an array of jet-like structures, while the legs of the inner horseshoe vortex appear to merge such that a stretched vortex ring is now formed. A schematic of this model is presented.

INTRODUCTION

In the case of a plane, stationary surface, Lighthill (1963) has shown that the surface vorticity flux, $\boldsymbol{\sigma}$, is simply related to surface pressure gradients. Their measurement has been shown by Andreopoulos and Agui (1996) to provide an accurate non-intrusive estimate of $\boldsymbol{\sigma}$. In simulations of turbulent channel flow, Koumoutsakos (1997, 1999) has used the surface pressure gradient as the basis of a simple, but efficient algorithm to control $\boldsymbol{\sigma}$. This can lead to a significant reduction in momentum flux and hence drag. In the case of a non-planar surface with finite relative acceleration, the generation of $\boldsymbol{\sigma}$ becomes more complicated with several mechanisms identified by Wu and Wu (1993, 1996):

$$\boldsymbol{\sigma} = -\nu(\mathbf{n}.\nabla\boldsymbol{\omega})_{\mathrm{w}} = -\boldsymbol{n}\times\boldsymbol{a} - \boldsymbol{n}\times\frac{\nabla p}{\rho} + \left(\boldsymbol{n}\times\frac{\tau_{\mathrm{w}}}{\rho}\right)\cdot\nabla\boldsymbol{n} - \boldsymbol{n}\left(\boldsymbol{n}\cdot\left(\nabla\times\frac{\tau_{\mathrm{w}}}{\rho}\right)\right) \quad (1)$$

in which the first, second and third terms on the right-hand side represent source terms of tangential vorticity due to, respectively, surface acceleration, $\boldsymbol{a}$, surface pressure gradient, and surface curvature, $-\nabla\boldsymbol{n}$, where $\boldsymbol{n}$ is the unit normal vector (inward-pointing). Wu and Wu (1996) call these three terms "ascending mechanisms". The last term shows how surface-normal vorticity arises effectively due to the solenoidal condition. Wu and Wu (1996) refer to this term as an "upturning mechanism". For a plane surface with in-plane acceleration, (1) provides two components of wall vorticity flux:

$$\sigma_z = -\nu\frac{\partial\omega_z}{\partial y} = a_x + \frac{1}{\rho}\frac{\partial p}{\partial x} \quad (2)$$

$$\sigma_x = \nu\frac{\partial\omega_x}{\partial y} = a_z + \frac{1}{\rho}\frac{\partial p}{\partial z} \quad (3)$$

The purpose of the present work is to investigate the effectiveness of time-dependent surface depressions ("dimples") as on-demand vortex generators that are part of a continuous surface. In laminar channel or laminar boundary layer flow, we examine the problem of local, time-dependent forcing by comparing the effect of changes in the viscous timescale, the timescale of the forcing, and the convective timescale. This may be posed more succinctly as a comparison of the effects of changes in both Reynolds number, Re_D, (based on freestream or centre-line velocity, U, and dimple diameter, D) and Strouhal number, $St = fD/U$, where f is the forcing frequency. Experimental work, primarily flow visualization, is used to investigate the effect of increasing St for a fixed amplitude, $0.1D$, at fixed Re_D. Simulations use a linearized boundary condition so that the effects of separation are precluded and fluid-structure interaction is neglected. In both cases, the dimple operates exclusively as a time-dependent depression: 'top-dead centre' occurs when the dimple is flush with the adjacent surface.

Alternative vortex generators such as "synthetic jets" (see, for example, Cater and Soria 2003) are operated by driving a diaphragm underneath an orifice with a periodic voltage so that it oscillates at its resonant frequency producing no net mass flow out of the orifice, yet generating a net momentum flux into the boundary layer by the process of non-linear streaming (Riley 2001). However there are many practical drawbacks to using synthetic jets, including the difficulty of controlling the actuation frequency, speed of response, and the most evident danger of ingesting dust (Lockerby *et al.* 2002). Lockerby and Carpenter (2004) have also noted that the diaphragm can be excited by a cavity resonance even when the device is inactive. In the context of heat transfer enhancement, the effect of static surface depressions has been studied by Isaev and Leont'ev (2003) and Mahmood *et al.* (2001). The fluid response to forcing by both these and synthetic jets can

be represented by (1), and in that sense, we take the term dimple to be a generalization of all types of local, time-dependent forcing, with or without surface discontinuities.

SIMULATIONS

Fully-attached flow over a time-dependent sinusoidally-shaped dimple in fully-developed laminar channel flow is simulated using the spectral/*hp* element code of Karniadakis and Sherwin (1999) with periodic boundary conditions in the spanwise (z) direction. Velocity boundary conditions for the dimple are developed using the linearized perturbation method of Gaster *et al.* (1994) imposed on the lower wall, $y = 0$. The dimple 'amplitude' varies sinusoidally in both x and z; it also has a sinusoidal variation in time.

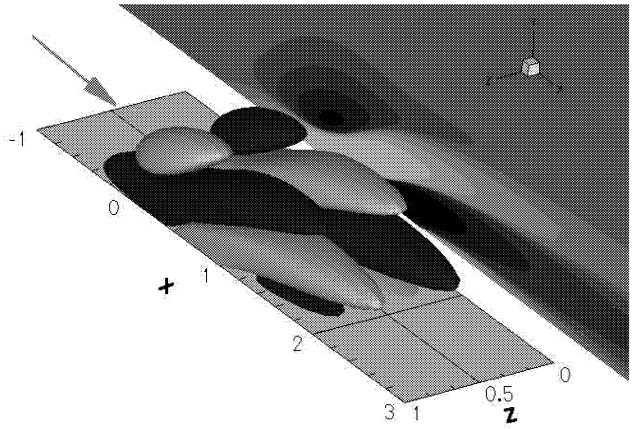

Figure 1: Contours of streamwise vorticity, ω_x: static dimple $St = 0$. Eight Fourier modes in spanwise direction. Light and dark shading denote opposite-signed vorticity: contour levels $\pm 2 \times 10^{-5} U/D$.

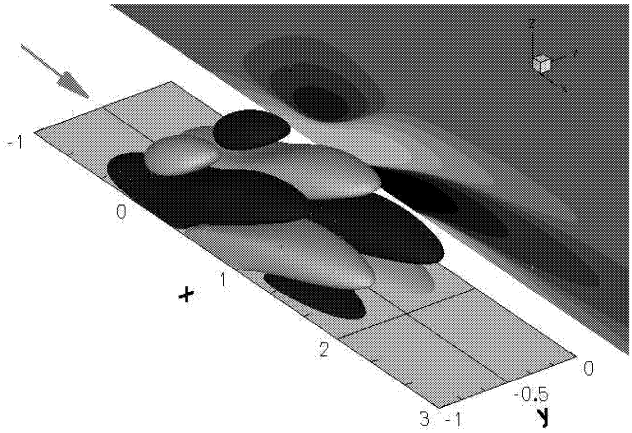

Figure 2: Contours of streamwise vorticity, ω_x: static dimple $St = 0$. 3D spatial resolution. Light and dark shading denote opposite-signed vorticity: contour levels $\pm 2 \times 10^{-5} U/D$.

Figures 1 and 2 show the generation of streamwise vorticity, ω_x, by a static dimple with dimple amplitude $\epsilon/D = 10^{-3}$ and $Re_D = 625$. Here, surface pressure gradients alone are responsible for the generation of ω_x which changes sign in both the streamwise and spanwise directions in conformity with the changes in pressure gradient. Figure 1 uses eight spanwise Fourier modes in the spanwise direction while figure 2 uses spatial discretization only.

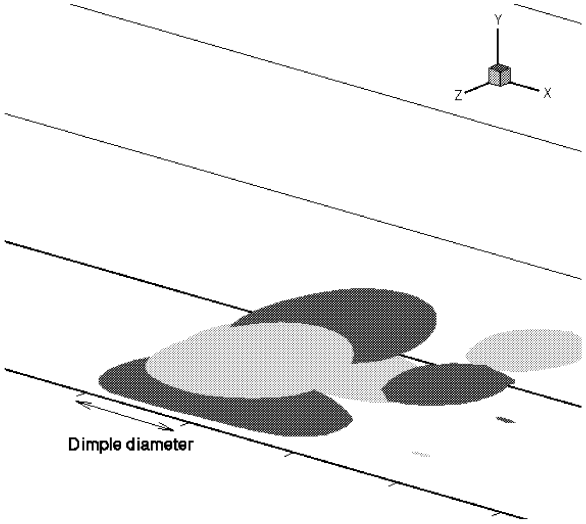

Figure 3: Contours of streamwise vorticity, ω_x: $St = 0.1$. Eight Fourier modes in spanwise direction. Light and dark shading denote opposite-signed vorticity: contour levels $\pm 2 \times 10^{-7} U/D$.

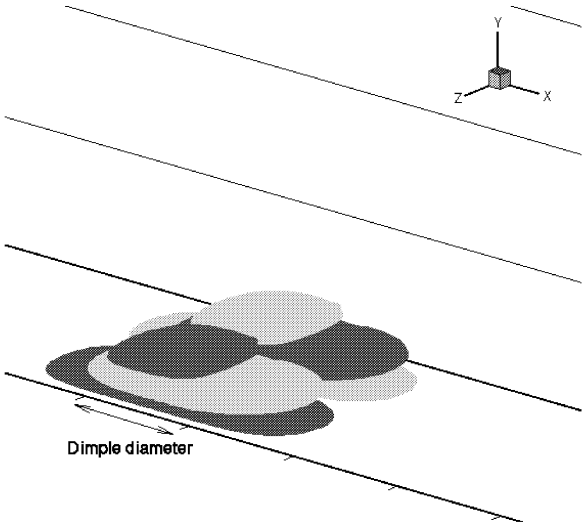

Figure 4: Contours of streamwise vorticity, ω_x: $St = 1.0$. Eight Fourier modes in spanwise direction. Light and dark shading denote opposite-signed vorticity: contour levels $\pm 2 \times 10^{-7} U/D$.

Figures 3 and 4 also show contours of ω_x, and compare the effects of a tenfold increase in forcing frequency, St. Here, the dimple amplitude is $\epsilon/D = 5 \times 10^{-6}$, with the ratio of dimple diameter to channel half-height, $D/H = 0.4$ and $Re_D = 100$. At $St = 0.1$, (figure 3) perturbations are convected downstream at the same time as growing away from the dimple owing to the dimple-induced flux and viscous diffusion. At $St = 1.0$, (figure 4) perturbations remain local to a narrow perturbed layer over the actuation period owing to the reduced effects of convection within one dimple cycle. At $St = 0.1$, unlike the velocity field of Stokes's second problem, the velocity field time-averaged over one period (not shown)

is non-zero – the result of non-linear effects. Figure 5 shows the period-averaged vorticity field, also for $St = 0.1$ (note that the contour levels remain the same), and it is indistinguishable from the equivalent pressure-gradient-driven, static case. At $St = 0.1$, the surface pressure gradient is the dominant mechanism in the generation of ω_x in which $\partial w/\partial y$ is by far the larger term with $\partial v/\partial z \approx 0$. At $St = 1.0$, a much larger contribution to the generation of ω_x comes from the dimple acceleration which is roughly in phase with spanwise pressure gradients. ω_x is still dominated by $\partial w/\partial y$, but $\partial v/\partial z$ now has a non-negligible contribution.

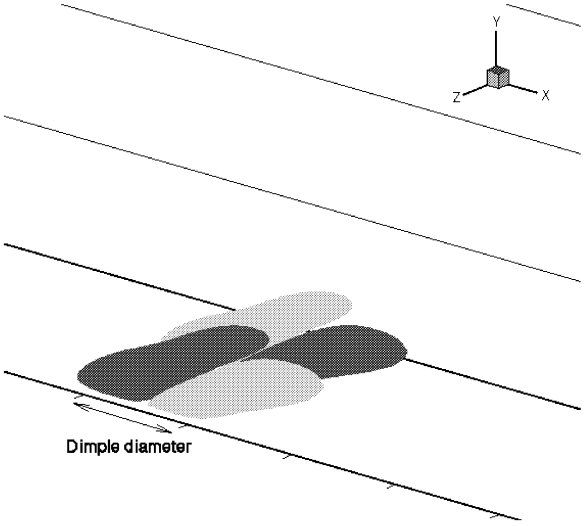

Figure 5: Contours of streamwise vorticity, ω_x: $St = 0.1$, averaged over one cycle. Eight Fourier modes in spanwise direction. Light and dark shading denote opposite-signed vorticity: contour levels $\pm 2 \times 10^{-7} U/D$.

At $St = 0.1$, streamwise vorticity contours on parallel planes close to the wall show that regions of maximum vorticity develop in the downstream half of the dimple, and then move upstream during the subsequent half of the dimple cycle, with new regions of opposite-signed vorticity appearing in the downstream half of the dimple, roughly in correspondence with the change in sign of the acceleration. When St is increased to 1.0, a single pair of 'lobes' of opposite-signed vorticity is present throughout most of the cycle, the generation terms now being dominated by the surface acceleration which dominates the pressure-gradient effects. This phenomenon is not inconsistent with the formation of a horseshoe vortex observed in the flow visualization experiments which do not preclude the effects of separation.

EXPERIMENTAL RESULTS

The flow visualization is performed in a water channel with a free surface at $Re_D = 400$ with a ratio of boundary layer thickness to dimple diameter of 2.4. The dimple model is positioned on the centre-line of the channel, 1.5m downstream of the start of the test section. It consists of a small piston, 16 mm in diameter, driven over a range of frequencies, $6.5 \leq St \leq 56$. $\epsilon/D = 0.1$ and separation is clearly evident. The Froude number is 0.12 so that free-surface effects can be ignored. Visualization is performed using potassium permanganate dye mixed with corn syrup and methanol, in a ratio of 1:2:1, to form a thick paste placed in a lump upstream of the dimple such that the dye is uniformly distributed across its face.

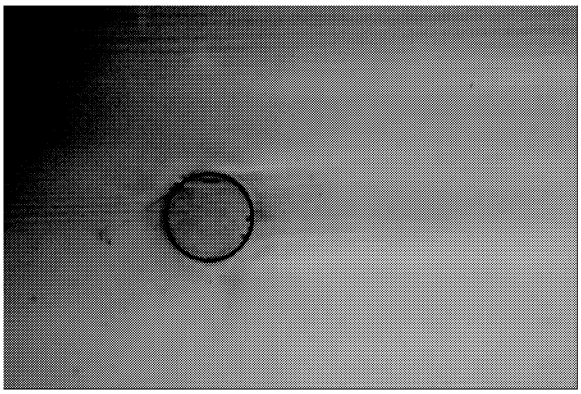

Figure 6: Plan view, flow from left to right, $St = 6.5$

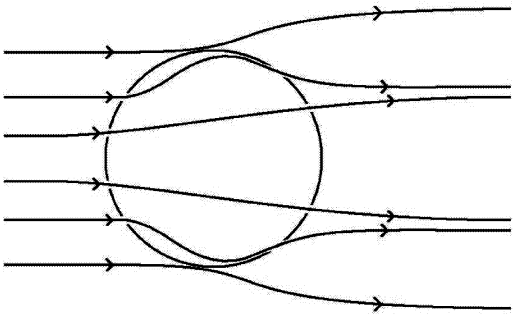

Figure 7: Sketch of streaklines over dimple face, $St = 6.5$

At each frequency, the flow visualization is first shown followed by an interpretation of the streaklines. Note that this amounts to a time-averaged view of the physical processes (streamlines), although some of the interpretation relies on differentiating the effects of the upstroke and downstroke of the dimple.

At low frequency, Figures 6 and 7 ($St = 6.5$) suggest that the behaviour is similar to that of flow over a static dimple with a similar amplitude. However, there are distinct effects caused by the upstroke and downstroke of the dimple face. The former results in the ejection of fluid so that streaklines diverge away from the horizontal streamwise centre-line. Conversely, the downstroke causes fluid to be sucked down into the upstream half of the dimple. Hence the streaklines in Figure 7 are consistent with the formation of a weak horseshoe vortex (common flow away from the solid surface at the centre-line).

At $St = 12$ (Figures 8 and 9), the horseshoe vortex is evident with outboard streaklines drawn in towards the centre-line and inboard streaklines pushed away from it. This corresponds to a pair of counter-rotating streamwise vortices centred on the chained lines (Figure 9) which are slightly inboard of the dimple perimeter, again with common flow away from the solid surface at the centre-line. Note that in the case of a static dimple with separation, streamwise vortices are formed by the influence of surface pressure gradients only, again with common flow away from the solid surface at the centre-line. It may therefore be concluded, that at this frequency, the generation of vorticity flux by pressure gradients still dominates that due to the dimple acceleration.

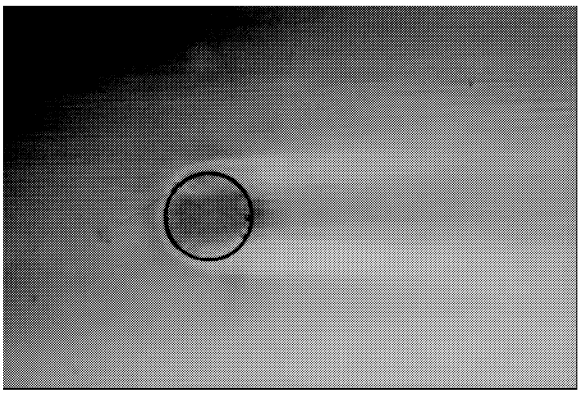

Figure 8: Plan view, flow from left to right, $St = 12$

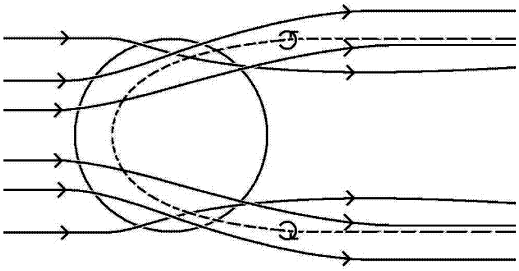

Figure 9: Sketch of streaklines over dimple face, $St = 12$.

At $St = 23$, there is a significant change (figures 10 and 11): a new horseshoe vortex is clearly evident, but now slightly upstream of the dimple and with a circulation such that it rotates in the opposite sense to the inner one already identified. Its rotation is consistent with an increased viscous blockage caused by the increase in forcing frequency. It also shows signs of an instability on its upstream surface which wrinkles and even shows signs of beginning to break up. This phenomenon occurs at a Reynolds number based on the dimple maximum velocity of about 1000, in common with the growth of waves on conventional laminar vortex rings. Streaklines upstream of the horseshoe vortex now clearly lift up away from the surface. As they approach the dimple face however, on the downstroke they are sucked down into the dimple cavity, while on the upstroke, the same fluid is pumped upward. Some of the fluid emerges as a jet-like ejection beneath the horseshoe vortex while the rest is ejected initially vertically to set up the inner, counter-rotating horseshoe vortex inside and immediately above the dimple cavity. Outboard streaklines are drawn towards the centre-line while inboard ones are pushed away from it. Figure 11 now shows (chained lines) two counter-rotating horseshoe vortices. The outer one, generated immediately upstream of the dimple, arises due to the viscous blockage that the dimple generates and has common flow towards the surface outboard and either side of the inner horseshoe vortex. The inner one is attributable to the dimple acceleration which reaches a maximum at each extreme of the dimple stroke. This generates common flow away from the solid surface, as seen at lower frequencies.

With further increases in frequency, this picture essentially remains unchanged. However two features in particular become more pronounced. The first, is shown in Figure 12 ($St = 34$), which now suggests that the upstream edge of the outer horseshoe vortex has broken up into distinct jet-like ejections. Their appearance becomes progressively more distinct as the dimple forcing frequency increases, figure 14 ($St = 45$) and figure 15 ($St = 56$). The second is somewhat more speculative: figure 13 now shows that the steamwise legs of the the inner horseshoe vortex have merged. This requires the generation of coherent spanwise vorticity and appears to be related to the onset of the production of a vortex ring by the dimple during its upstroke. This effect is likely to be more pronounced at higher frequencies, but unfortunately, more detailed interpretations are not possible at higher frequencies with the present experimental arrangement.

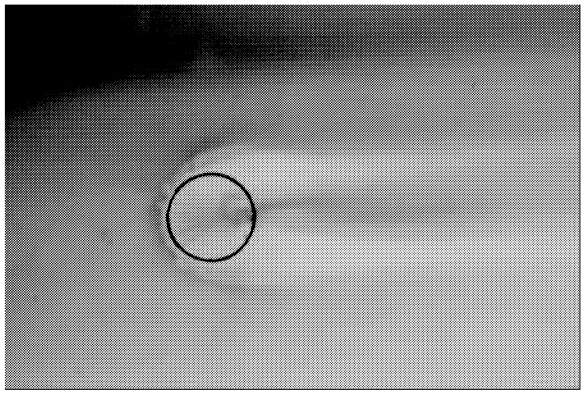

Figure 10: Plan view, flow from left to right, $St = 23$.

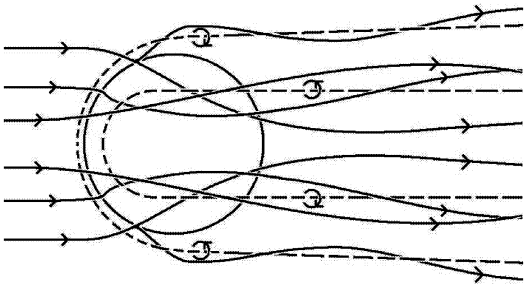

Figure 11: Sketch of streaklines over dimple face, $St = 23$.

DISCUSSION AND CONCLUSIONS

The basic mechanisms by which a local time-dependent surface deformation cam generate a flux of vorticity has been illustrated. Key to this is the large increase in streamwise vorticity caused by the surface acceleration which, practically speaking, may be controlled straightforwardly by the use of an appropriate actuator. This suggests that the penetration length (as defined by Cater and Soria 2002) can be easily controlled and this is unlikely to be the case for a synthetic jet of fixed geometry and operating at its resonant frequency. Therefore it seems likely that a dimple actuator is a promising candidate as an on-demand vortex generator, that is, one that provides a vortex of known circulation for a prescribed duration at the required location. Present designs of dimples produce counter-rotating pairs of vortices and a design refinement is required to produce vortices singly.

Future work will involve fully resolved simulations of the dimple motion without the need for linearized boundary conditions so that the effects of separation in and around the

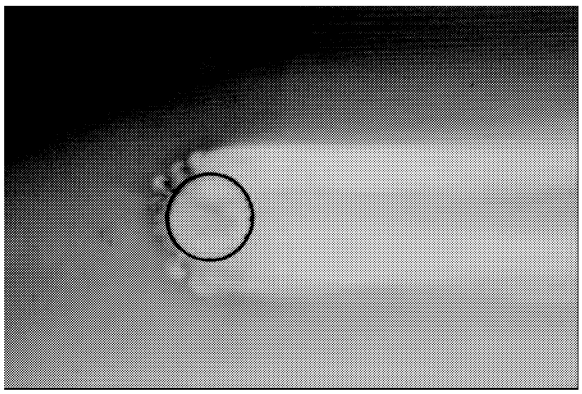

Figure 12: Plan view, flow from left to right, $St = 34$.

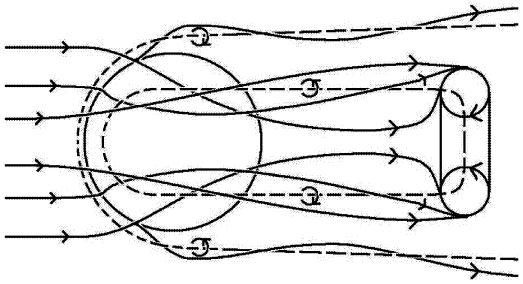

Figure 13: Sketch of streaklines over dimple face, $St = 34$.

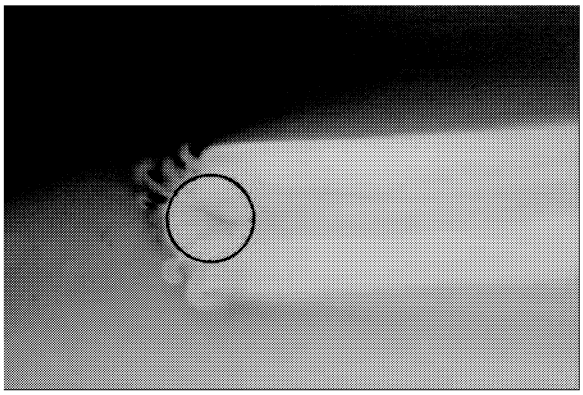

Figure 14: Plan view, flow from left to right, $St = 45$.

dimple can be simulated. Further simulations are required to examine the effect of the fluid/dimple coupling. Future experimental work will involve investigation of the time-dependent features of dimple forcing using PIV measurements of dimple motion in laminar boundary layers. Kelso and Smits (1995) have noted that, even when a steady jet emerges into a laminar boundary layer, the horseshoe vortex motion can be steady, oscillatory or coalescing, depending on the flow conditions. For the present work, a time-dependent topological analysis (Perry and Chong 1987) is clearly called for. Given that (1) includes a curvature generation term, further work also includes an examination of the effect of different dimple profile shapes. Subsequent investigations will be extended to an analysis of dimple interactions with a turbulent boundary layer.

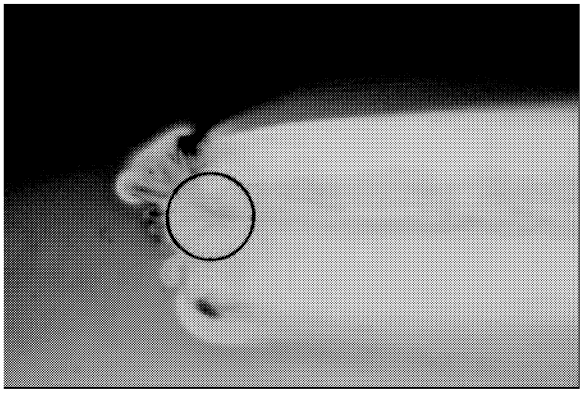

Figure 15: $St = 56$.

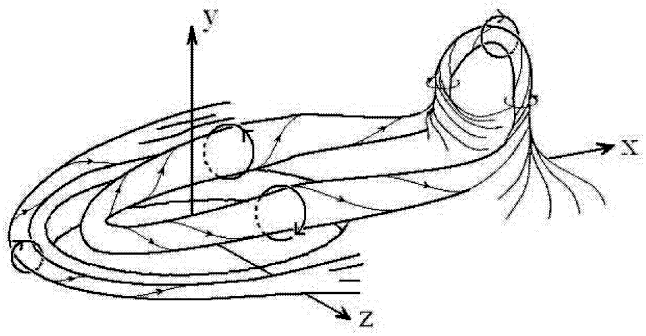

Figure 16: Schematic of model for high frequencies, $St > 20$.

Acknowledgments

This work was supported by the Engineering and Physical Sciences Research Council under grant GR/S20994. We are grateful to Spencer Sherwin for access to, and his assistance with the spectral/*hp* finite element code. BJM is a Royal Society Dorothy Hodgkin Fellow.

REFERENCES

Andreopoulos, J., and Agui, J. H., 1996, "Wall-vorticity flux dynamics in a two-dimensional turbulent boundary layer", *J. Fluid Mech.*, Vol. 309, pp. 45–84.

Cater, J. E., and Soria, J., 2002, "The evolution of round zero-net-mass-flux jets", *J. Fluid Mech.*, Vol. 472, pp. 167–200.

Gaster, M., Grosch, C. E., and Jackson, T. L. 1994, "The velocity field created by a shallow bump in a boundary layer", *Phys. Fluids*, Vol. 6, pp. 3079–3085.

Isaev, S. A., and Leont'ev, A. I., 2003, "Numerical simulation of the vortex enhancement of heat transfer under conditions of turbulent flow past a spherical dimple on the wall of a narrow channel", *Teplofiz. Vys. Temp.*, Vol.41(5), pp. 775–770.

Karniadakis, G. E., and Sherwin, S. J., 1999, "*Spectral/hp Element Methods for Computational Fluid Dynamics*", Oxford University Press.

Kelso, R. M., and Smits, A. J., 1995, "Horseshoe vortex systems resulting from the interaction between a laminar boundary layer and a transverse jet", *Phys. Fluids*, Vol. 7, pp. 153–158.

Koumoutsakos, P., 1997, "Active control of vortex-wall interactions", *Phys. Fluids*, Vol. 9, pp. 3808–3816.

Koumoutsakos, P., 1999, "Vorticity flux control for a turbulent channel flow", *Phys. Fluids*, Vol. 11, pp. 248–250.

Lighthill, M. J., 1963, "Introduction. Boundary layer theory", in *Laminar Boundary Layers*, L. Rosenhead, ed., Dover Publications Inc.

Mahmood, G. I., Hill, M. L., Nelson, D. L., Ligrani, P. M., Moon, H.-K., and Glezer, B., 2001, "Local heat transfer and flow structure on and above a dimpled surface in a channel", *J. Turbo.*, Vol. 123, pp. 115–123.

McKeon, B. J., Lambert, S., Sherwin, S. J., and Morrison, J. F., 2004, "Active dimples for flow control", *Advances in Turbulence X. Proceedings, 10th European Turbulence Conference*, H. I. Andersson & P. Å. Krogstad, ed., CIMNE, Barcelona, pp. 581–584.

Perry, A. E., and Chong, M. S., 1995, "A description of eddying motions and flow patterns using critical point concepts", *Annu. Rev. Fluid Mech.*, Vol. 19, pp. 125–155.

Riley, N., 2001, "Steady streaming", *Ann. Rev. Fluid Mech.*, Vol. 33, pp. 43–65.

Wu, J.-Z., and Wu, J.-M., 1993, "Interactions between a solid surface and a viscous compressible flow field", *J. Fluid Mech.*, Vol. 254, pp. 183–211.

Wu, J.–Z., and Wu, J.–M., 1996, "Vorticity dynamics on boundaries", *Adv. Appl. Mech.*, Vol. 32, pp. 119–275.